

Fe II Diagnostic Tools for Quasars

E. Verner^{1,2,3} and F. Bruhweiler^{1,2,4}

D. Verner^{1,5}

S. Johansson⁶

T. Kallman⁷

T. Gull^{2,8}

ABSTRACT

The enrichment of Fe, relative to alpha-elements such as O and Mg, represents a potential means to determine the age of quasars and probe the galaxy formation epoch.

To explore how Fe II emission in quasars is linked to physical conditions and abundance, we have constructed a 830-level Fe II model atom and investigated through photoionization calculations how Fe II emission strengths depend on non-abundance factors. We have split Fe II emission into three major wavelength bands, Fe II (UV), Fe II(Opt1), and Fe II(Opt2), and explore how the Fe II(UV)/Mg II, Fe II(UV)/Fe II (Opt1) and Fe II(UV)/Fe II (Opt2)

¹IACS/Dept. of Physics, Catholic University of America.

²Laboratory of Astronomy and Solar Physics, NASA/Goddard Space Flight Center Greenbelt MD 20771.

³email: kverner@fe2.gsfc.nasa.gov

⁴email: fredb@iacs.gsfc.nasa.gov

⁵email: verner15@comcast.net

⁶Lund Observatory, Lund University, P.O. Box 43, S-22100 Lund, Sweden, Sveneric.Johansson@astro.lu.se

⁷Laboratory for High Energy Astrophysics, NASA Goddard Space Flight Center, Greenbelt, MD20771, timothy.r.kallman@nasa.gov

⁸email: theodore.r.gull@nasa.gov

emission ratios depend upon hydrogen density and ionizing flux in broad-line regions (BLR’s) of quasars. Our calculations show that: 1) similar Fe II(UV)/Mg II ratios can exist over a wide range of physical conditions; 2) the Fe II(UV)/Fe II (Opt1) and Fe II(UV)/Fe II (Opt2) ratios serve to constrain ionizing luminosity and hydrogen density; and 3) flux measurements of Fe II bands and knowledge of ionizing flux provide tools to derive distances to BLR’s in quasars. To derive all BLR physical parameters with uncertainties, comparisons of our model with observations of a large quasar sample at low redshift ($z < 1$) is desirable.

The STIS and NICMOS spectrographs aboard the Hubble Space Telescope (HST) offer the best means to provide such observations.

Subject headings: atomic processes—line: formation—methods: numerical—quasars: emission lines

1. Introduction

The observed ratio of restframe Fe II UV emission from 2200–3000 Å (thereafter, Fe II(UV)) to that of the Mg II 2800 Å resonance doublet has been widely used to estimate Fe/Mg abundance ratios in BLRs of quasars (Wills et al. 1985, thereafter WNW85; Iwamuro et al. 2002; Dietrich et al. 2002, 2003; Freudling et al. 2003; Barth et al. 2003; Maiolino et al. 2003). Iron enrichment is not expected in evolution scenarios at redshifts $z \leq 1$ (Hamann & Ferland 1993; Yoshii et al. 1996; Heger & Woosley 2002). Meanwhile, there is some observational evidence that narrow line AGN have higher metallicities compared to other low redshift AGN (Shemmer & Netzer 2002).

Measurements of Fe II(UV)/Mg II emission ratios in quasars show large scatter from 1 to 20, and no redshift dependency up to $z \sim 6.4$ (Iwamuro et al. 2002).

In a recent paper, we have used a sophisticated 830-level model for Fe II to investigate abundance and microturbulence effects on these ratios (Verner et al. 2003a). Our modeling indicates strong Fe II emission from 1000 to 6800 Å, and reveals that Fe II (UV)/Mg II ratios (at $n_H = 10^{9.5} \text{ cm}^{-3}$ and total hydrogen column density $N_H = 10^{24} \text{ cm}^{-2}$) increase from 5 to 30 for microturbulence v_{turb} varied from 1 to 100 km s⁻¹, while an increase in abundance by factor 10 only increases the same ratios by factor 2. We have further found that a reasonable range of microturbulence is between 5–10 km s⁻¹, and Fe II optical emission flux from 4000–6000 Å is more sensitive to abundance than is the Fe II(UV) band. Conversely, the Fe II(UV) band is more sensitive to microturbulence than the Fe II optical band.

In this paper we continue our study of Fe II emission line formation in BLRs of quasars in an attempt to explain the nature of the large observed scatter. Since abundances, density, and excitation conditions are ill-determined in BLRs, we have performed a set of numerical calculations to study the effects of varying hydrogen and ionizing photon densities. We have split Fe II emission into three wavelength bands that are most commonly measured in observations: Fe II(UV) (2000–3000 Å), Fe II(Opt1) (3000–3500 Å), and Fe II(Opt2) (4000–6000 Å). The major goal is to ascertain if Fe II(UV)/Mg II, Fe II(UV)/Fe II(Opt1), and Fe II(UV)/Fe II(Opt2) emission ratios present different trends due to non-abundance factors.

Although many factors contribute to increase Fe II emission fluxes, the effects can be separated by using several ratios simultaneously. Spectra of quasars at redshifts up to $z = 1$ are especially valuable, since they should exhibit no elemental overabundances, and the effects of physical parameters such as hydrogen density, ionizing luminosity, and even microturbulence can be easily explored. We just showed general trends, while a detailed comparison between model and observations for each quasar spectrum should be done individually. The figures in our paper represent calculations for a range of reasonable BLR conditions, but do not cover the full range of possible variables and should be used with extreme care by observers. Such comparison will provide the first fundamental test of the Fe II emission model. This consistency check is a necessary step before one can confidently apply this methodology to quasars over a wide range of redshift as a means to probe galactic chemical evolution models. The required data for quasars up to $z = 1$ can be obtained with STIS and NICMOS aboard the HST.

2. Non-abundance Effects and BLR Diagnostic Based on Fe II Emission

Why quasars at moderate to high redshift exhibit strong UV Fe II emission is one the unsolved problems of AGN studies. The extremely complex energy level structure (Johansson 1978) of Fe II makes it very difficult to obtain all the experimental transition probabilities and, therefore, calculate line intensities. Several hundreds of transitions of Fe II must be considered, many with large optical depths. Our earlier model for Fe⁺ included 371 energy levels below 11.6 eV (Verner et al. 1999), which was incorporated into photoionization code CLOUDY (Ferland et al. 1998). Even though the upper energy levels in the current model (Verner et al. 2003a) have been extended only about 2.5 eV higher compared to the old model, the total number of transitions has increased dramatically from 68,638 to 344,035. The model includes 830 levels up to 14.1 eV. This increase in transitions is mainly due to increased density of energy levels at higher energy. The energy level data are from Johansson

(2004).

The large number of Fe II lines form several distinct emission bands recognized in early observational work (e.g. Greenstein & Schmidt 1964; Wampler & Oke 1967; Sargent 1968; Netzer & Wills 1983) and theoretical modeling (WNW85; Verner et al. 1999). The 830-level ion model is far more accurate than the previous best efforts. The increased number of Fe⁺ energy levels influences not only the Fe II spectrum but also the whole energy budget, temperature, and consequently line emission of other elements in the emitting region. However, an in-depth study of the new theoretical emission spectrum will not be given in this paper.

For several reasons, we have followed a more general approach and considered three wide Fe II bands in our calculations, namely Fe II (UV), Fe II (Opt1), and Fe II (Opt2). The biggest unknown factor in predicting Fe II (UV) and Mg II emission is the magnitude of the velocity of turbulence in BLRs. Whether it is on the order of 10 km s⁻¹, 100 km s⁻¹ or even higher is not at all clear (Alexander & Netzer 1997; Murray & Chiang 1997). Also, the Fe II emission in BLRs is present over a wide wavelength range from 1000 Å to the IR. Because of the velocity broadening, presumably due to orbital motion, the Fe II emission can be characterized by a pseudo-continuum superposed upon the intrinsic power-law spectrum of the quasar.

For the adopted parameter range, we have investigated how hydrogen density and photon density of hydrogen ionizing photons at the illuminated face alter the intrinsic emission ratios of Fe II(UV)/Mg II, Fe II (UV)/Fe II(Opt1) and Fe II (UV)/Fe II(Opt2). For our calculations, we have used the same Fe II energy level structure and model as in Verner et al. (2003a). We have looked for the variations of Fe II(UV)/Mg II emission ratios in BLRs assuming solar abundance for a wide range of hydrogen density, $n_H = 10^{9.5} - 10^{13.0} \text{ cm}^{-3}$, and total column density, $N_H = 10^{24} \text{ cm}^{-2}$. We further assume that the flux of hydrogen ionizing photons at the illuminated face is $10^{17.5} - 10^{22.0} \text{ cm}^{-2} \text{ s}^{-1}$. These parameters for BLR conditions are within the range of values taken from Verner et al. (1999) and Verner (2000). We employ the characteristic AGN continuum described in Korista et al. (1997), which consists of a UV bump peaking near 44 eV, a $f_\nu \propto \nu^{-1}$ X-ray power law, and a UV to optical spectral index, $a_{ox} = -1.4$.

Our knowledge about turbulence is very limited. Consequently, in our initial calculations of Fe II emission, we have produced models with microturbulence with velocities of $v_{turb} = 0, 5, 10, \text{ and } 100 \text{ km s}^{-1}$. We find that the strength of the Fe II(UV) emission is very sensitive to microturbulence. Non-zero turbulence velocities help to explain the observed smooth shape of Fe II(UV), and a $v_{turb} = 5 \text{ km s}^{-1}$ makes the model fit reasonable (Verner et al. 2003b) Fe II emission strengths forming a pseudo-continuum (Figure 1) at $v_{turb} = 5 \text{ km s}^{-1}$. Even in emission lines, this must be a curve-of-growth effect.

Stronger lines (higher A-values) should have larger equivalent width and be more sensitive to microturbulence than weaker lines.

Figure 2 shows plots of Fe II(UV)/Mg II ratios versus hydrogen density and flux of ionizing photons at $v_{turb} = 0, 5, \text{ and } 10 \text{ km s}^{-1}$.

We see from Figure 2 that at low flux, $\Phi < 10^{19.0} \text{ cm}^{-2} \text{ s}^{-1}$, the Fe II(UV)/Mg II ~ 1 and it does not depend on turbulent velocity. The increase of microturbulence works similar to a hydrogen density increase, and large Fe II(UV)/Mg II ratios are predicted at smaller densities.

Although solar abundance is assumed throughout, the possible range of values of Fe II(UV)/Mg II are quite large, from 1 to 40 (Fig. 2, $v_{turb} = 5 \text{ km s}^{-1}$). Fig. 2 also demonstrates that the same Fe II(UV)/Mg II ratios may indicate a wide range of physical conditions. At densities below $n_H = 10^{11.0} \text{ cm}^{-3}$, the dependence on luminosity displays a different trend compared to that at larger densities. The Fe II(UV)/Mg II ratio reaches a maximum near $n_H = 10^{10.0} \text{ cm}^{-3}$. In quasars, if hydrogen density is less than $n_H = 10^{11.0} \text{ cm}^{-3}$, all Fe II(UV)/Mg II values are less than 8. Small Fe II(UV)/Mg II ratios (up to 2) are possible indicators of two different regimes: a) high luminosity conditions at small densities ($n_H \leq 10^{11.0} \text{ cm}^{-3}$) or b) low-luminosity conditions over a wide density range. In the latter case, these ratios are insensitive to density variations. The left upper corner in Figure 2 corresponds to low hydrogen density and large ionizing flux, and shows that iron and magnesium are effectively more highly ionized, beyond Fe II and Mg II. The large ionizing flux at high hydrogen density is insufficient to ionize Fe II. Instead, this combination increases the strength of the Fe II(UV) emission band relative to the Mg II doublet emission. As a result, large Fe II(UV)/Mg II ratios (from 8 to 40) are predicted for large hydrogen density $n_H = 10^{11.0} - 10^{13.0} \text{ cm}^{-3}$ and ionizing fluxes $10^{20.5} - 10^{22.0} \text{ cm}^{-2} \text{ s}^{-1}$. If the scatter observed at any given redshift is due to variations in density and luminosity, it may well mask any abundance effect.

As we have already shown (Verner et al. 2003a), the Fe II(UV)/Fe II(Optical) ratio is less sensitive to microturbulence velocity than is the Fe II(UV)/Mg II ratio. Figures 3 and 4 illustrate this conclusion for both ratios, namely Fe II(UV)/Fe II(Opt1) and Fe II(UV)/Fe II(Opt2).

Figure 3 shows how the Fe II(UV) and Fe II(Opt1) emission varies versus physical conditions at $v_{turb} = 0, 5, \text{ and } 10 \text{ km s}^{-1}$. If $v_{turb} = 5 \text{ km s}^{-1}$, the Fe II(UV)/Fe II(Opt1) ratios vary from ~ 1 to 30. However, there is a wide plateau with almost constant Fe II(UV)/Fe II(Opt1) ratio 6–7. At low ionizing flux with increasing density, Fe II(UV) dominates over Fe II(Opt1). Ratios ≥ 8 show a dependence on physical conditions and are more suitable to use as a diagnostic of ionizing photon flux and hydrogen number density.

The Fe II(UV)/Fe II(Opt2) ratios exhibit a much stronger dependence on density than either Fe II(UV)/Mg II or Fe II(UV)/Fe II(Opt1). The plateau where ratios are insensitive to physical conditions is much smaller than that in the previous case. Similarly, the Fe II(UV) dominates over Fe II(Opt2) emission strength in the domain of high density and low ionizing flux (Fig. 4 at $v_{turb} = 5 \text{ km s}^{-1}$).

The Fe II bands include different Fe II transitions. The Fe II(UV) band includes the strongest UV multiplets from UV1 to UV5. The Fe II(Opt1) band includes optical multiplets 1, 4-7 and Fe II(Opt2) optical multiplets 21, 22, 25, 27, 28, 35-38. UV multiplets are due to transitions from higher energy upper levels compared to those of the optical multiplets. Therefore, UV multiplets become stronger with increasing density due to increase of upper level populations, and Fe II(UV)/Fe II(Opt1), Fe II(UV)/Fe II(Opt2) ratios become larger.

While no single ratio can constrain physical conditions, their combination can provide valuable diagnostics of density and ionizing flux. If our assumption about microturbulence is correct, we might well observe large Fe II(UV)/Mg II values (> 10) at solar abundance. For the same physical conditions, Fe II(UV)/Fe II(Opt1) ratios will be in a range of 5 – 10 and Fe II(UV)/Fe II(Opt2) in a range of 7 – 15. Likewise, large scatter in Fe II(UV)/Mg II, from 1 to 30, can be explained by non-abundance factors, where both ionizing luminosity and hydrogen density are responsible. Values of Fe II(UV)/Mg II ≥ 10 are most probably achieved at hydrogen densities, larger than $n_H = 10^{11.0} \text{ cm}^{-3}$ at high ionizing flux.

It is highly desirable to develop an observational template to derive Mg/Fe abundances. Yet, it is not clear that any single template can be constructed that would be appropriate for all quasar spectra. A combined observational and detailed modeling program is needed to determine the answer to this question. Currently, two types of Fe II templates have been used. One template is based upon the I ZW 1 spectrum (e.g. Vestergaard & Wilkes 2001; Dietrich et al. 2002, 2003) and the other is based on an average quasar template (WNW85, Iwamuro et al. 2002). Our comparisons between model and observations reveal that the I ZW 1 template by Vestergaard & Wilkes (2001) is not generally applicable to BLRs due to variable Fe II emission contributions contaminating measurements of the Mg II doublet. The contributions of Fe II lines are easily seen in our modeling of BLRs. Failure to account for this Fe II contamination to the Mg II emission can lead to erroneous Mg II emission estimates. Assuming $\log \Phi_{ion} = 20.5$, the values of Fe II (2720 – 2860 Å)/ Mg II are 1.3, 0.8 and 0.2, for $n_H = 10^{11} \text{ cm}^{-3}$, 10^{12} cm^{-3} , and 10^{13} cm^{-3} , respectively. Thus, errors in the Mg II flux can be of factor 2 and even higher, if the contribution of Fe II lines is not accounted for. Naturally, the larger measured Fe II (UV)/ Mg II ratio the more Mg II affected by the Fe II emission (Fig. 5).

The emission spectrum of Fe II in BLRs spans a wide wavelength range from the UV

to IR. It affects not only line intensity measurements of other ions, but the continuum determinations as well. Based on the model predictions, it is possible to define a narrow ($\sim 20 \text{ \AA}$) Fe II window in quasar spectra near $3,050 \text{ \AA}$, where little or no Fe II emission is present. In case of the strong Fe II(UV) band, the emission produces a pseudo-continuum that extends to wavelengths as short as $1,000 \text{ \AA}$. How much the Fe II(UV) pseudo-continuum affects the $1,000 \text{ \AA} - 2,000 \text{ \AA}$ range, depends on microturbulence and hydrogen density, and is the subject of future investigation. If any of these Fe II windows are used to determine the underlying quasar continuum, it must be done with caution.

In most studies of quasars, even at low redshift, Fe is thought to have super-solar abundances. WNW85 were the first who recognized that ultraviolet Fe II emission contributed to Mg II resonance doublet. However, in their analysis they still needed an iron overabundance of approximately 3 times solar to explain the high Fe II(UV)/Mg II ratios. From comparisons of Figures 2 – 4 we can deduce the physical conditions in BLRs. The ionizing flux at the face of the cloud is $\Phi_{ion} = L_{ion}/4\pi r^2$, where L_{ion} is total ionizing luminosity. Since we can easily estimate the ionizing luminosity from observations, we can calculate the number of ionizing photons at any distance from the central source, and hence obtain a distance for the BLR from the central engine.

We selected five objects from WNW85 with measured Mg II and Fe II(UV), Fe II(Opt1), and Fe II(Opt2) emission bands. We then compared these measurements with Figures 2–4 to deduce hydrogen densities and ionizing photon fluxes for the BLRs of the quasars. Finally, we have ascertained if enhanced Fe abundances are required to explain the observations. Where possible, we have used the values corrected for intrinsic and foreground reddening. The results are given in Table 1. Column 1 shows the name of the object, where the three following columns present the observed emission ratios similar to that calculated in our model. The next two columns list hydrogen densities and ionizing photon fluxes. The last two columns give photon luminosities and derived sizes of emitting regions.

When we compare these results with the WNW85 models, we find no iron overabundance at redshifts $0.15 < z < 0.7$. The best fits are obtained within reasonable hydrogen densities, $10^{10.0} - 10^{13.0} \text{ cm}^{-3}$. The much larger number of Fe II levels used in the photoionization calculations provides more sensitivity to the radiation field, and enables us to explain the much larger observed Fe II(UV)/Mg II ratios.

Quasar luminosities were derived from energy fluxes measured by the ASCA X-ray observations (the Tartarus database; Turner & Nandra, <http://tartarus.gsfc.nasa.gov/>) for Q0405–123 and Q1226+023, and from the Rosat radio loud catalog (Brinkmann et al. 1997) for the remainder of the objects. These were converted into 0.0136–10 keV number fluxes using the power law indices, and then into number photon luminosity assuming $H_0 = 71$

km s⁻¹ Mpc⁻¹ (Bennett et al. 2003) and $q_0 = 1$. Note that derived hydrogen densities vary by factor 1000 from one quasar to another. Yet there is a wide range of ionizing luminosities. Meanwhile all derived distances of the Fe II emitting region vary by only factor of 6. Is it something common for all quasars, or are these distances fortuitously similar to each other only in this small sample? Future reverberation mapping results for quasars over a range of luminosity would provide important comparison with the model predictions (c.f. Kaspi et al. 2000, hereafter K2000). We have one quasar in common with the K2000 sample, namely PG 1226. Its BLR distance based on reverberation method is ≈ 7 times larger than that in our model. Note that the large distance for PG 1226 is not typical for quasars in the K2000 sample, contrary to the distance derived in our model. On the other hand, the source for the discrepancy between the R found in our work for PG1226+023 and that obtained from reverberation mapping in K2000 may be quasar variability.

We have used our sample just for demonstration purposes and assumed a constant $v_{turb} = 5$ km s⁻¹ for all quasars. By varying v_{turb} we can achieve even better agreement between the observed and predicted Fe II(UV)/Mg II ratios without any iron overabundance (Verner et al. 2003a).

3. Summary

By applying our new 830-level model for Fe⁺ ion, which is incorporated into detailed photoionization calculations, we have probed the feasibility of using the strong Fe II emission spectrum seen in quasars as a diagnostic tool for the physical conditions in BLRs. The Fe II emission ratios show different trends as functions of the same parameters, hydrogen number density, and ionizing photon flux. We have found that the combination of the ratios is especially important in determining the hydrogen density, the ionizing flux and the radial distances to BLRs in quasars. We conclude that abundance is not the only factor that makes Fe II emission strong. Moreover, Fe abundance does not seem to be the dominant factor determining the strength of Fe II emission. Our modeling indicates that microturbulence, density, and radiation field have important roles and also lead to preferential strengthening of the Fe II UV emission.

On the basis of the calculations presented here, we have three main conclusions:

1. Our Fe II large model atom used in photoionization calculations predicts that large Fe II(UV)/Mg II ratios are not necessarily due to high iron abundance. The Fe II(UV)/Mg II diagram (Figure 2) demonstrates that the Fe II(UV)/Mg II ratios can have the same value over a wide range of physical conditions. This implies that the averaging of large numbers

of quasars spectra may lead to properties of quasars that do not exist.

2. Since evolutionary models predict no iron overabundances for $z \leq 1$, observations to detect the optical iron band at these redshifts will be beneficial to calibrate the model assuming a solar abundance for iron. Such research must be accomplished with STIS and NICMOS aboard the HST to properly span the wavelength range where Fe II emission is seen and to obtain constraints on the most uncertain parameter, microturbulence.

3. Our Fe II emission band analysis demonstrates that Fe II has a great potential for becoming an important diagnostic tool of the physical conditions in BLR's of quasars. We suggest three Fe II emission ratios, which can be used to obtain hydrogen density, flux of hydrogen-ionizing photons, microturbulent velocities, and distances to BLR's.

In this paper we have shown that even in the limited space of parameters (ionizing flux and hydrogen density) exact fits to observed spectra exist. The full investigation of our model in the whole parameter space including dust properties, Balmer continuum, and many others will be a subject of coming papers. Such investigation will provide all BLR physical parameters with the determined uncertainties.

The research of EV has been supported through an NSF grant (NSF - 0206150) to CUA. SJ is supported by a grant from the Swedish National Space Board. We wish to acknowledge the use of the computational facilities of the Laboratory for Astronomy and Solar Physics (LASP) at NASA/Goddard Space Center. We give special thanks to Keith Feggans, Don Lindler, and Terry Beck for their computer services support. We are grateful to unknown referee for helpful comments.

REFERENCES

- Alexander, T., & Netzer, H. 1997, MNRAS, 284, 267
- Barth, A., Martini, P., Nelson, C. H., & Ho, L. C. 2003, ApJ, 594, 95
- Bennett et al. 2003, ApJS, 148, 1
- Brinkmann, W., Yuan, W., & Siebert, J., 1997 A&A, 319, 413
- Dietrich, M., Appenzeller, I., Vestergaard, M. ., & Wagner, S. J. 2002, ApJ, 564, 581
- Dietrich, M., Hamann, F., & Vestergaard, M. 2003, ApJ, 596, 817
- Ferland, G. J. et al. 1998, PASP, 110, 761

- Freudling, W., Corbin, M., & Korista, K. 2003, ApJ, 587, L67
- Greenstein, J., & Schmidt, M. 1964, ApJ, 140, 1
- Hamann, F., & Ferland, G. 1993, ApJ, 418, 11
- Heger, A., & Woosley, S. E. 2002, ApJ, 567, 532
- Iwamuro, F., Motohara, K., Maihara, T., Kimura, M., Yoshiii, Y., & Doi, M. 2002, ApJ, 565, 63
- Johansson, S. 1978, Physica Scripta, 18, 217
- Johansson, S. 2004, preliminary database, Lund Observatory
- Kaspi, S. et al. 2000, ApJ, 565, 63
- Korista, K., Baldwin, J., Ferland, G., & Verner, D. 1997, ApJS, 108, 401
- Maiolino, R., Juarez, Y., Mujica, R., Nagar, N. M., & Oliva, E. 2003, ApJ, 596, 155
- Murray, N. & Chiang, J. 1997, ApJ, 494, 91
- Netzer, H., & Wills, B. 1983, ApJ, 275, 445
- Sargent, W. 1968, ApJ, 152, L31
- Shemmer, O. & Netzer, H. 2002, ApJ, 569, L59
- Verner E. M., Verner, D. A., Korista, K.T., Ferguson, J. W., Hamann, F., & Ferland, G. J. 1999, ApJS, 120, 101
- Verner, E., 2000, Ph.D. thesis, Univ. of Toronto
- Verner, E., Bruhweiler, F., Verner, D., Johansson, S., Gull, T., 2003, ApJ, 592, L59
- Verner, E., Bruhweiler, F., Tsuzuki, Y., Kawara, K., Yoshii, Y., Oyabu, S. 2003, BAAS, 203, 78.15
- Vestergaard, M. & Wilkes, B.J., 2001, ApJS, 134, 1
- Wample, E. & Oke, J., 1967, ApJ, 148, 695
- Wheeler, J. C., Sneden, C., & Truran, J. W. 1989, ARA&A, 27, 279
- Wills, B. J., Netzer, H., & Wills, D. 1985, ApJ, 288, 94

Yoshii, Y., Tsujimoto, T., & Nomoto, K., 1996, ApJ, 462, 266

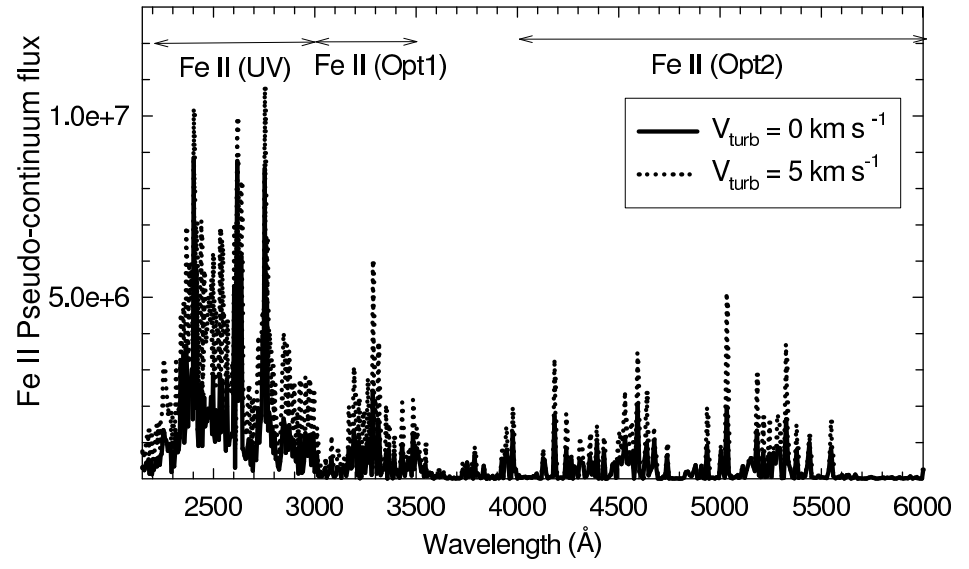
Fig. 1.— Fe II pseudo-continuum predicted by 830-level Fe⁺ model for physical conditions in QSO BLRs. The 2200–6000 Å wavelength range is divided into small bins of 6 Å (consistent with a ~ 500 km s⁻¹ FWHM at 3600 Å) and Fe II flux calculated in each bin. The model at $v_{turb} = 0$ km s⁻¹ predicts many strong and narrow Fe II features in the 1600–3500 Å range (solid line). The same model, but at $v_{turb} = 5$ km s⁻¹ is marked by dashed lines.

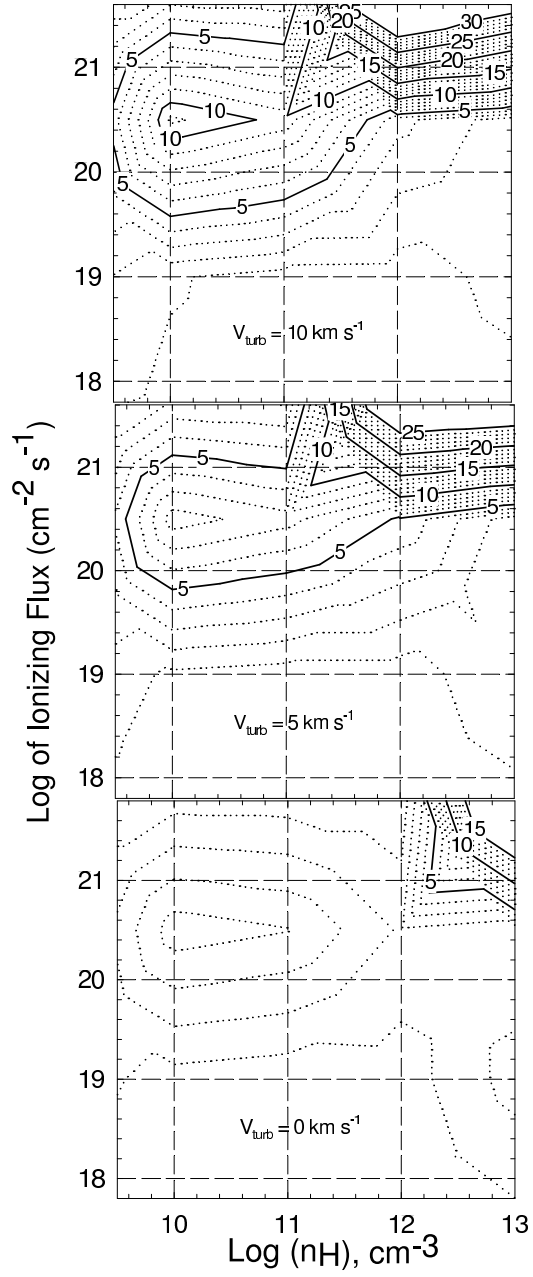
Fig. 2.— The Fe II(UV)/Mg II ratios predicted using 830-level model for Fe⁺ in a QSO BLR as a function of the hydrogen density n_H and flux of hydrogen-ionizing photons. The chemical abundances are solar, the cloud column density is 10^{24} cm⁻³, and $v_{turb} = 0, 5,$ and 10 km s⁻¹.

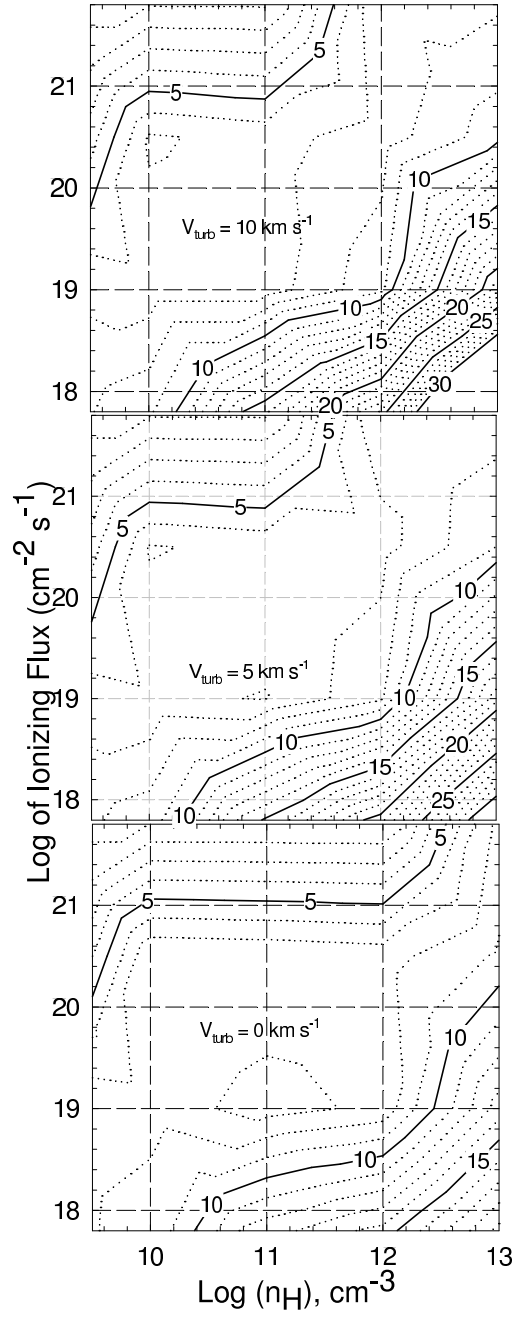
Fig. 3.— The predicted Fe II(UV)/Fe II(Opt1) ratios calculated for the same parameters as in Figure 2.

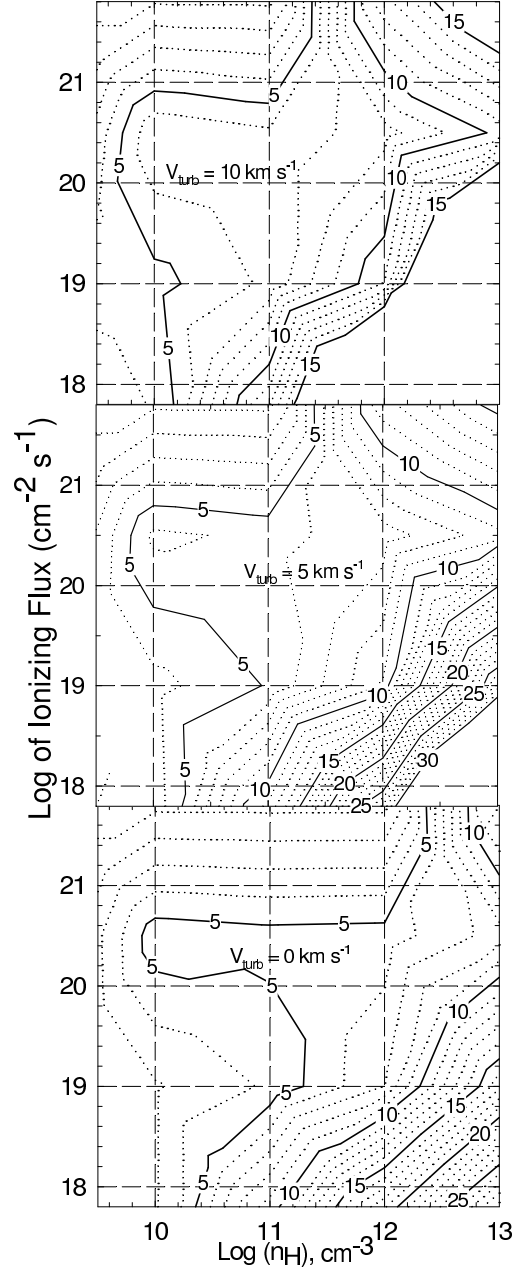
Fig. 4.— The predicted Fe II(UV)/Fe II(Opt2) ratios calculated for same parameters as in Figure 2.

Fig. 5.— Contribution of Fe II to Mg II doublet, Fe II(2720–2860Å)/Mg II, $v_{turb} = 5$ km s⁻¹.









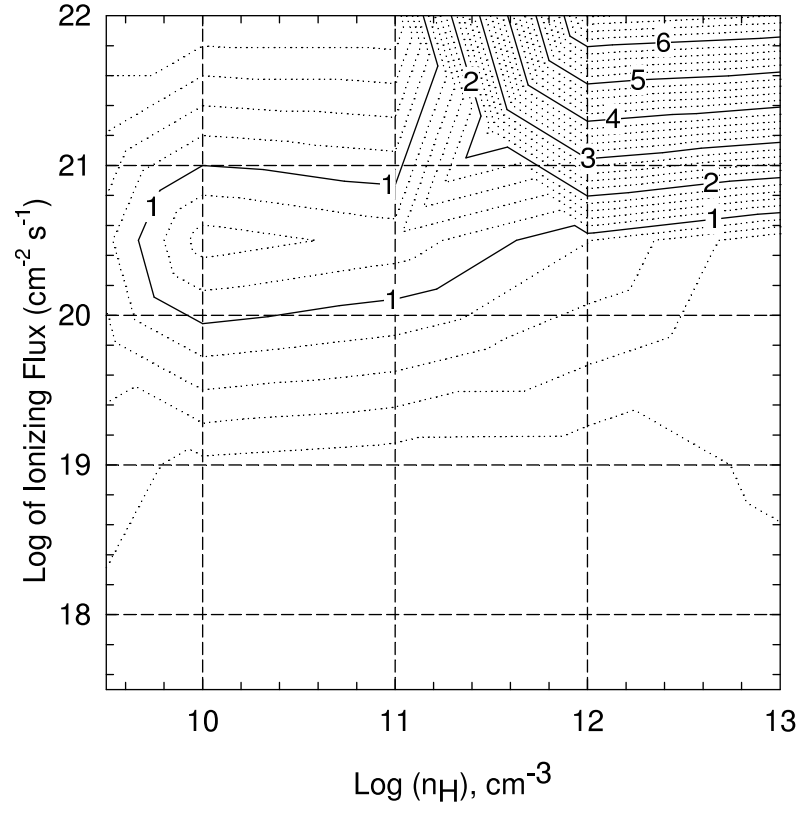


Table 1. Predicted Hydrogen Densities, Ionizing Fluxes, & Distances to BLRs.

Object	WNW85			This work			
	$\frac{\text{FeII(UV)}}{\text{MgII}}$	$\frac{\text{FeII(UV)}}{\text{FeII(Opt1)}}$	$\frac{\text{FeII(UV)}}{\text{FeII(Opt2)}}$	$\log n_H$ cm^{-3}	$\log \Phi_{ion}$ $\text{cm}^{-2} \text{ s}^{-1}$	L^b $10^{56} \text{ photons s}^{-1}$	R 10^{17} cm
1	2	3	4	5	6	7	8
0405–123	8	7.7	4	10	20.6	7.47	3.86
0738+313	5.4	5.0	4.8	10	21	5.08	2.01
0742+318 ^a	6.1	13.2	8	13	20.5	.57	1.20
1104+167	6.0	4.8	9.5	11.5	20.5	17.4	6.62
1226+023 ^a	9.8	6.8	4.7	11.5	21.5	7.33	1.36

^a Intensities have been corrected due to intrinsic reddening.

^b Photon luminosity in 0.0136–10 keV range. See also text for details.